Bioorg. Med. Chem. 134 (2026) 118542

Contents lists available at ScienceDirect

Bioorganic & Medicinal Chemistry

journal homepage: www.elsevier.com/locate/bmc

Targeting microbial β-CAs: bridging *in silico* screening with *in vitro* validation

Anna Rita Tondo [a,1], Marialuigia Fantacuzzi [b,1], Simone Carradori [b,c], Ilaria D'Agostino [d], Andrea Angeli [e], Claudiu T. Supuran [e], Clemente Capasso [f], Nicola Gambacorta [a], Luca Piemontese [a], Antonio Laghezza [a], Orazio Nicolotti [a], Paolo Tortorella [a,*], Mariangela Agamennone [b,*]

[a] Department of Pharmacy and Pharmaceutical Sciences, University of Bari "A. Moro", Via Orabona 4, 70126 Bari, Italy
[b] Department of Pharmacy, "G. d'Annunzio" University of Chieti-Pescara, via dei Vestini 31, 66100 Chieti, Italy
[c] UdA-TechLab, "G. d'Annunzio" University of Chieti-Pescara, via dei Vestini 31, 66100 Chieti, Italy
[d] Department of Pharmacy, University of Pisa, via Bonanno Pisano 6, 56126 Pisa, Italy
[e] NEUROFARBA Department, Pharmaceutical and Nutraceutical Section, University of Florence, via Ugo Schiff 6, 50019 Sesto Fiorentino, Italy
[f] Department of Biology, Agriculture and Food Sciences, CNR, Institute of Biosciences and Bioresources, via Pietro Castellino 111, 80131 Napoli, Italy

ARTICLE INFO

Keywords:
Antibacterial
Antimicrobial resistance
Virtual screening
β-carbonic anhydrases
Repurposing approach
Induced fit docking
Pseudomonas aeruginosa

ABSTRACT

Antimicrobial resistance (AMR) is one of the world's most pressing health problems and requires immediate action from the scientific community. *Pseudomonas aeruginosa* is a particularly concerning bacterium due to its high level of resistance, especially among hospitalized and immunocompromised individuals. We recently investigated PsCA3, one of three *P. aeruginosa* β-carbonic anhydrases (β-CAs), as a potential new pharmacological target for developing innovative antibacterial drugs. In this study, we applied a consensus structure-based virtual screening approach to select the most promising PsCA3 inhibitors from an in-house library of 607 small molecules. Twenty-one diverse compounds were selected and experimentally validated through enzyme inhibition assays, which assessed the ability of all ligands to block PsCA3 activity while sparing human α-carbonic anhydrases (*h*CAs). Next, we focused on the benzoxazinone/dihydroquinolinone scaffold, testing fifteen additional analogues and expanding the set of assayed microbial β-CAs. Notably, we identified new, potent ligands based on unexplored scaffolds that can effectively target microbial β-CAs at micromolar/submicromolar concentrations with remarkable selectivity over human CAs.

1. Introduction

Antimicrobial resistance (AMR) is one of the major global health threats that is increasing rapidly due to the widespread misuse of antibiotics in human medicine and livestock production. Recent epidemiological reports estimate that AMR was associated with 4.95 million deaths in 2019, a number expected to rise significantly in the coming decades.[1,2] Addressing this challenge requires complementary strategies, including prudent antibiotic use, surveillance programs, and the development of compounds acting through alternative mechanisms of action.[3,4] Accordingly, major international initiatives, such as Combating Antibiotic Resistant Bacteria Biopharmaceutical Accelerator (CARB-X), are accelerating the search for innovative antibacterial therapies.[5] Progress in deciphering resistance mechanisms, including enzymatic inactivation, target alteration, decreased permeability, efflux enhancement, and metabolic reprogramming, is providing crucial insights for new countermeasures.[6] Current efforts are therefore pursuing both optimized antibiotics for established targets and new small molecules with genuinely novel modes of action.

β-CAs have emerged as promising alternative antimicrobial targets.[7] They belong to the large carbonic anhydrases (CAs) superfamily (EC 4.2.1.1), which includes eight classes (α, β, γ, δ, ζ, η, θ, and ι) expressed in all living organisms.[8] Despite their structural diversity, all CAs catalyze the reversible hydration of CO_2 to HCO_3^-, and H^+, an essential reaction for acid-base balance and pH regulation. In bacteria, CAs support crucial processes such as CO_2 fixation, pH homeostasis, energy

* Corresponding authors.
E-mail addresses: paolo.tortorella@uniba.it (P. Tortorella), mariangela.agamennone@unich.it (M. Agamennone).
[1] These authors contributed equally to this work.

https://doi.org/10.1016/j.bmc.2025.118542
Received 20 October 2025; Received in revised form 19 December 2025; Accepted 22 December 2025
Available online 27 December 2025

generation, and metabolic adaptation.[9] Bacterial genomes typically encode α-, β-, γ-, and ι-CAs, whereas humans express only α-class enzymes, enabling opportunities for selective inhibition. β-CAs play established roles in bacterial survival and virulence: PsCA1 of *Pseudomonas aeruginosa* contributes to calcium deposition; CynT from *Escherichia coli* is essential for growth at atmospheric CO_2; and β-CA from *Helicobacter pylori* is required for periplasmic urease function.[10–14] Several selective β-CAs inhibitors have been identified and shown to be effective against various pathogens (Fig. 1),[10,15,16] including antibiotic-resistant strains like *Vancomycin-Resistant Enterococci* and *Neisseria gonorrhoeae*.[17] Furthermore, the combination of β-CA inhibitors with other antimicrobial agents has shown synergistic effects that enhance overall antimicrobial efficacy.[18]

Over the past few years, we have studied several microbial β-CAs and developed structure-based computational models to unveil the rationale behind their inhibition and binding.[15,19] Most recently, we investigated PsCA3, a β-CA expressed by *P. aeruginosa*,[20] a common Gram-negative opportunistic pathogen which is responsible for life-threatening nosocomial infections and, along with *Enterococcus faecium, Staphylococcus aureus, Klebsiella pneumoniae*, *Streptococcus pneumoniae* and *Acinetobacter baumannii*, is a member of the ESKAPE pathogens.[21] The World Health Organization (WHO) reported that *P. aeruginosa* is on the list of priority bacterial pathogens for 2024 and stressed the need for new research to reduce the impact of carbapenemase-resistant *P. aeruginosa* (CRPA) due to its high mortality rate among immunocompromised people and in healthcare settings.[22]

P. aeruginosa encodes for three β-CAs, namely PsCA1, PsCA2, and PsCA3, and three γ-CAs. PsCA3 is a specialized, type II β-CA, functioning mainly under alkaline conditions (pH > 8) to regulate CO_2 and bicarbonate levels which is critical for biosynthetic processes in bacteria.[23] It is a structurally characterized β-CA with limited sequence similarity with PsCA1 and PsCA2 (almost 40%). PsCA3 represents a promising target for new antimicrobials, with inhibitor studies showing proof-of-concept for selective bacterial growth suppression.[24]

We employed our recent knowledge on PsCA3 in the search for new effective β-CA inhibitors. To this end, we screened a small *in-house* library of compounds synthesized over the years with different purposes. The combination of structure-based virtual screening and experimental testing allowed the identification of effective compounds. Our ultimate goal was to find new scaffolds that can effectively address the design of novel antimicrobial β-CA inhibitors.

2. Materials and methods

2.1. Chemical compounds

Tested compounds were already published in reference articles (see Section 3.4). The characterization data of the main tested compounds, along with their ^{1}H NMR spectra, are provided in the Supplementary Material.

2.2. Computational studies

2.2.1. Virtual library collection and preparation

All compounds from the *in-house* library were reported as SMILES strings, along with their IDs, positions in the lab, and remaining quantities. The initial dataset of 776 structures was carefully reviewed to remove duplicates, resulting in a final dataset of 607 unique compounds. The library was then submitted to the LigPrep module of the Schrödinger Suite v2021-2, which generated 3D structures for each compound at physiological pH.[25] Chirality was retained where specified; in the other cases, stereoisomers were generated.

2.2.2. Structure-based virtual screening on PsCA3

The prepared compound library was subjected to structure-based virtual screening against PsCA3 using a consensus docking approach. As a first step, the coordinates of the tetrameric X-ray structure of PsCA3 in complex with the sulfamide cognate ligand (PDB code: 6D2N)[26] were downloaded from the Protein Data Bank (PDB)[27] and converted to a dimer using PyMOL.[28]

Structural optimization of the X-ray structure was performed using the Protein Preparation Wizard in the Schrödinger Suite.[25] This procedure includes recovery of missing side chains, determination of protonation states at pH 7.4 ± 0.0, removal of water molecules, and constrained minimization of the entire structure using the OPLS4 force field.[29]

The in-house compound library was subjected to eight Glide SP docking protocols[25,30,31] with different settings as described below. Based on favorable docking results previously reported by Marinacci et al.,[20] the first two docking protocols used the protein obtained from an Induced Fit (IF) docking,[25] which was previously applied to the most active compounds in the series. A 35 Å grid box centered on residues Tyr99, Arg105, Glu141, Asp145, Gly183, and Lys185, which together define the "selective valley",[26] was set up; other default docking parameters were maintained (docking protocol 1) or a metal constraint on Zn^{2+} was added (docking protocol 2).

The previously prepared protein from PDB was used in additional protocols that vary because of the position and the dimension of the grid box, along with the presence or absence of the metal constraint as summarized in Table 1.

For each docking protocol, five poses per ligand were generated and ranked according to the SP docking score. The top 5 % of docking poses were extracted from each of the eight ranked structures: two new consensus ranks based on docking score and ligand efficiency were generated, and the most promising compounds were selected by visual inspection.

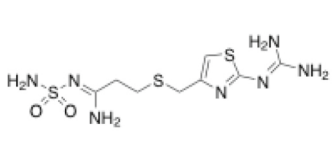

Famotidine[16]

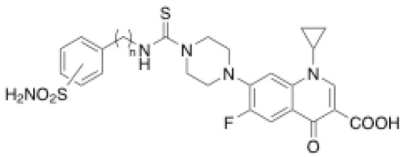

A[20]

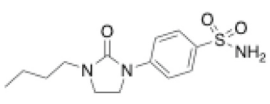

B[19]

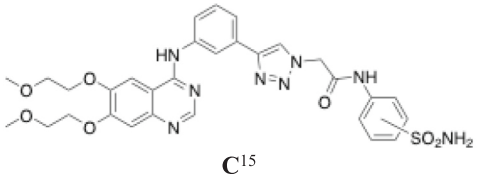

C[15]

Fig. 1. Representative inhibitors of β-CAs.

Table 1
Parameters applied in the eight docking protocols used for virtual screening. The origin of the 3D structure, the center and position of the grid box, and the presence of the metal constraint on the zinc ion are reported.

Protocol n	Structure	Center of the grid box	Dimension of the grid box (Å)	Zn^{2+} metal constraint
1	IF-derived	Selective valley	35	No
2	IF-derived	Selective valley	35	Yes
3	PDB original	Zinc ion	30	Yes
4	PDB original	Zinc ion	30	No
5	PDB original	Selective valley	35	Yes
6	PDB Original	Selective valley	35	No
7	PDB original	X-ray ligand	30	Yes
8	PDB original	X-ray ligand	30	No

An estimation of free energies (ΔG) of binding between protein and active ligands were performed for the twenty-one selected compounds and the set of fifteen analogues using the Molecular Mechanics/Generalized Born Surface Area (MM-GBSA) method[32] implemented in the Prime module of the Schrödinger suite; binding affinity estimation of the thirty-six molecules was performed for docking poses of all eight docking protocols.

2.2.3. Structure-based computational studies on microbial β-CAs

The crystal structures of *Burkholderia pseudomallei* (BpsCAβ) was retrieved from the Protein Data Bank (PDB code: 6YJN).[33] The 3D models of β-CAs form *Trichomonas vaginalis* (TvaCA1), *Streptococcus mutans* (SmuCA), *Malassezia restrictans* (MreCA), *Malassezia globosa* (MgCA), and *Mycobacterium tuberculosis* (MtbCA3) were obtained from the AlphaFold Protein Structure Database (IDs: AF-A2ENQ8, AF-Q8DVY1, AF-A0A3G2S4B9, AF-A8Q1N3, AF-P96878, respectively).[34,35] The 3D coordinates of *Vibrio cholerae* β-CA (VchCAβ) were obtained *via* homology modeling in a previous study[19]; the structure of the PgiCAβ from *Porphyromonas gingivalis* was generated by a similar procedure. The amino acid sequence of PgiCAβ (UniProt ID: A0A0K2J5Z9) was retrieved from the UniProt KnowledgeBase (UniProtKB) database[36] and used as a query sequence for homology modeling with Prime,[37] which uses BLAST[38] to identify suitable templates from the PDB. The resulting model of PgiCAβ was obtained using the structure of MtbCA2 (PDB code: 2A5V,[39] identity 36.55 %) as the template.

The single chain model was duplicated and aligned to each chain of the crystal structure of PsCA3 to obtain the homodimer structure. The crystallographic coordinates of the zinc ion, as obtained from the PDB structure of PsCA3 (PDB code: 6D2N), were incorporated into each βCA protein model. To adapt the protein structures to the tested ligands, the 3D coordinates of compound **9**, derived from the best docked pose on PsCA3, were integrated into each protein structure. The obtained protein-ligand complexes were minimized by employing MacroModel and applying the OPLS4 force field, executing 5000 steps of PRCG minimization with a convergence criterion of 0.05 kJ/mol Å, to optimize the residue positioning around the ligand. The correct coordination of the zinc ion by the two cysteine residues and the histidine of the active site was verified for all models.

Glide was used to generate the receptor grid based on the binding geometry of compound **9**, and the Ligand Docking tool[37] of Maestro was employed for conducting a molecular docking study in standard precision (SP) mode. In addition, the IF docking protocol[37] was applied to study the conformational changes experienced by the receptor in the presence of the selected ligand.

The SiteMap tool of Maestro[37] was employed to evaluate the active site properties of the microbial β-CAs. For all enzymes, the best-scoring ligand:enzyme complex obtained from the IF protocol was analyzed, evaluating the binding site and encompassing a region about the ligand plus a 5 Å buffer, using the less restrictive definition of hydrophobicity, a fine grid, and cropping site maps at 4 Å from the nearest site point.

2.3. Enzyme inhibition of microbial β-CAs and hCAs

A stopped-flow instrument from Applied Photophysics was used to measure CA-catalyzed CO_2 hydration activity.[40] Phenol red (at a concentration of 0.2 mM) was used as an indicator, working at an absorbance maximum of 557 nm, with 20 mM 4-(2-hydroxyethyl)-1-piperazine ethanesulfonic acid (HEPES) (pH 7.4 for α-CAs, pH 8.4 for β-CAs) as a buffer and 20 mM Na_2SO_4 (to maintain constant ionic strength) were used to follow the initial rates of the CA-catalyzed CO_2 hydration reaction for a period of 10–100 s. CO_2 concentrations ranged from 1.7 to 17 mM for the determination of kinetic parameters and inhibition constants. The enzyme concentrations ranged from 5 to 12 nM. For each inhibitor, at least six traces of the first 5–10 % of the reaction were used to determine the initial rate. The uncatalyzed rates were determined in the same manner and subtracted from the total observed rates. Stock solutions of inhibitor (0.1 mM) were prepared in distilled deionized water and then diluted to 0.01 nM with assay buffer. Inhibitor and enzyme solutions were preincubated together for 8 h at room temperature prior to the assay to allow formation of the *E*-I complex. Inhibition constants were obtained by nonlinear least squares methods using PRISM 3 and the Cheng-Prusoff equation as previously reported and represent the mean of at least three different determinations. Except for commercial *h*CAs I and II, all CA isoforms were home-made recombinant proteins as reported previously.[20,41,42]

3. Results and discussion

3.1. In-house library

A proprietary library comprising 607 distinct structures was employed to conduct a structure-based virtual screening. This library predominantly includes matrix metalloproteinase (MMP) inhibitors that have been synthesized within our laboratory over the years.[43–46] Noteworthy, these compounds contain typical Zinc Binding Groups (ZBGs) capable of engaging the catalytic zinc ion, which is also a key feature in the binding site of CAs. On the other hand, it is known that some MMP inhibitors can show efficacy against specific human α-CA isoforms (I, II, IX, XII, and XIV).[47–49] Nevertheless, to broaden the scope of the screening, the library incorporated additional compounds, including those with experimental annotations for various targets, such as Peroxisome Proliferator Receptor (PPAR),[50] Acetylcholinesterase,[51] and ATP-sensitive-K^+ (K_{ATP}) channels.[52,53]

3.2. Structure-based virtual screening

PsCA3 is a type II β-CA that functions at basic pH (8.3) and exists in a *closed* state in which the zinc ion is complexed by two histidine residues, one cysteine, and one aspartate as the fourth binder. Catalytic activation by displacement of the aspartate side chain is required for substrate-ligand binding.[54] Furthermore, the inspection of the available X-ray structures of PsCA3 reveals that the access to the catalytic zinc ion is quite narrow, thus preventing the entrance of inhibitors. Therefore, in the previous study, we employed an IF approach to favor the positioning of ligands in the binding site.[20] In the present case, given the structural diversity of our library, eight parallel docking calculations based on different settings were performed to get more accurate and reliable results. In particular, the original 3D coordinates taken from the PDB and the adapted structure resulting from the IF protocol were used. Other variables of the docking protocols were the position and dimension of

the grid box and the presence of the metal constraint on the catalytic zinc ion (Table 1). The grid box has been centered on either the zinc ion, the X-ray ligand, or the so-called *selective valley*. The latter is a region of PsCA3 defined by Murray as important for binding selective ligands and characterized by residues Tyr99, Arg105, Glu141, Asp145, Gly183, and Lys185.[26]

A consensus approach was employed to combine the results of the eight docking calculations to shortlist a preliminary set of best candidates to forward to *in vitro* studies. In that regard, the initial criterion adopted was based on selecting the top ten compounds provided with the overall best docking scores and *glide ligand efficiency* values. Then, all the selected compounds were subjected to further inspection to evaluate the quality of the binding poses and the sampling of different scaffolds. Using this approach, twenty-one compounds were finally selected (Table 2).

3.3. Enzyme inhibition assays

The panel of selected compounds was tested using enzyme inhibition assays on *h*CAs I, *h*CA II, and PsCA3 to evaluate their inhibitory effect on the target protein and their selectivity toward physiologically relevant isoforms I and II.

Micromolar/submicromolar activity was detected for all tested compounds (Table 2). Compared to AAZ, which is the reference standard for CA inhibition, all compounds showed lower potency against the target enzyme (PsCA3) and significantly higher selectivity over *h*CAs. The most active inhibitor was **12** with an K_I nearly 300 nM and promising isoform selectivity. The weaker inhibitor was found to be compound **4**, with an K_I of 4 μM.

It is noteworthy that all selected compounds showed conserved activity and selectivity despite their structural diversity. Considering the structural variability of known β-CA inhibitors (Fig. 1), this result is not surprising. Unlike our expectations, most of the newly identified CA inhibitors were not MMP inhibitors, except for bisphosphonates and pyrogallols.

To better rationalize the enzyme inhibition data, the best docked poses obtained from the eight different docking runs were refined using a MM-GBSA calculation. For instance, the optimized pose of the most active compound (**12**) from docking protocol 1 (Table 1) reveals that the pyridinic nitrogen coordinates the zinc ion and the same pyridine ring establishes a π–T interaction with Phe83 (Fig. 2). The same interactions (with the zinc ion and Phe83) are the most frequently retrieved in the docking poses of active compounds, suggesting that they play a key role in determining the inhibition of PsCA3.

3.4. Scaffold analysis and hit expansion

Building on these first results, we enlarged the pool of the selected candidates by including some analogues sharing the most promising scaffold. To this end, we considered the ligand efficiency related to PsCA3 inhibition and selectivity against *h*CAs, as well as the synthetic feasibility, chemical stability, and drug-likeness of active compounds (Table S1, Supplementary Material).

All tested and active compounds can be assigned to five main groups including: bisphosphonates (**4** and **5**), benzoxazine (**12**–**17**), benzoxazinones (**10**,**11**) and dihydroquinolinones (**8**, **9**), aryloxyalkanoic derivatives or their analogs (**1**–**3**), pyrogallols (**6**–**7**), and others (**18**–**21**).

Aryloxyalkanoic derivatives, along with their isosteres have been investigated as potential PPAR agonists.[55] We assessed an aryloxypropionic derivative **3** and two analogs **1** and **2**. These derivatives feature a straightforward and practical scaffold, exhibiting commendable activity, albeit slightly less potent than benzoxazine and benzoxazinones. Notably, their activity is maintained even with ester derivatives, despite β-CAs lack of detectable esterase activity, in contrast to other CAs.

Bisphosphonates have been widely acknowledged for their

Table 2
K_I values of selected compounds (represented as 2D structures) and reference compound acetazolamide (AAZ) on *h*CAs I and II, and PsCA3 through the stopped-flow CO_2 hydration assay.[40]

N	Structure	K_I (μM)[a] *h*CA I	*h*CA II	PsCA3
1	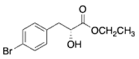	>100	53.1	0.96
2	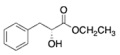	>100	>100	1.01
3	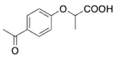	>100	>100	1.87
4		95.3	61.0	4.03
5		>100	>100	0.37
6	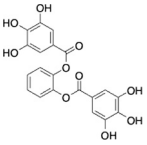	47.0	66.3	1.33
7	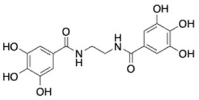	>100	74.0	1.41
8		>100	>100	1.06
9		>100	>100	0.90
10		>100	>100	1.15
11	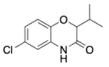	>100	92.5	0.91
12	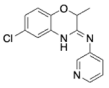	84.6	41.9	0.30
13	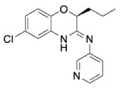	>100	>100	0.61
14	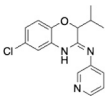	>100	>100	0.41
15	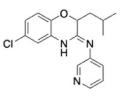	>100	>100	1.11
16	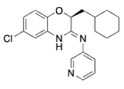	53.4	84.6	1.22

(*continued on next page*)

Table 2 (*continued*)

N	Structure	K_I (μM)[a] *h*CA I	*h*CA II	PsCA3
17	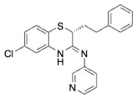	>100	>100	0.78
18	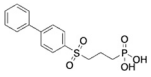	87.3	76.0	0.60
19	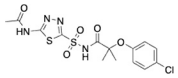	5.95	16.7	0.49
20	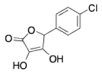	>100	>100	1383
21	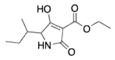	>100	5.02	1.26
AAZ		0.250	0.012	0.076

[a] Mean of three different assays by a stopped flow technique (errors were in the range of ±5–10 % of the reported values). Incubation: 8 h, r.t.

effectiveness in treating osteoporosis and, more recently, for inhibiting MMPs implicated in bone metastases.[45,56–58] In contrast to **4**, compound **5** exhibited significant activity and selectivity toward PsCA3. However, docking results indicated that **5** interacts with the zinc ion through its pyridine nitrogen, unlike the direct involvement of phosphonic acid observed in **4** or in the binding of the zinc ion in MMPs.[58] This divergence in binding modes raises concerns about establishing a consistent structure-activity relationship (SAR) for this series of compounds. Additionally, both compounds were excluded from further analogue selection due to their limited drug-likeness.

Pyrogalloles **6** and **7** have been explored as ZBGs in the development of MMP inhibitors.[45,59,60] However, owing to their recognition as frequent hitters in many biochemical high-throughput screenings[61] and to their rapid metabolism, we decided to prioritize alternative structures that may demonstrate lower promiscuity.

Benzoxazine derivatives (**12**–**17**) have been studied as modulators of skeletal muscle ATP-sensitive-K^+ channels (K_{ATP}).[52,53] Due to stability issues exhibited by these compounds and the requirement for fresh purification, we have decided, despite their promising activity, to exclude them from the following analogue selection. However, we are considering their intermediates: dihydroquinolinones (**8**, **9**) and benzoxazinones (**10**, **11**) that, moreover, have demonstrated micromolar activity against *h*CA I and *h*CA II.[62] The remaining compounds were excluded from following studies due to either low inhibitory potency or low isoform selectivity.

Based on previous analysis, compounds featuring the benzoxazinone scaffold stand out as promising candidates for further studies. This scaffold represents an intriguing structural framework due to its synthetic feasibility.[63] Consequently, a substructure search for the benzoxazinone/dihydroquinolinones scaffold was performed within the initial library, leading to the selection of fifteen analogues (Table 3) which were subsequently tested for enzyme inhibition against the same panel of CA isoenzymes. The enzyme activity curves for representative isoforms and compounds are reported in Fig. S1.

None of the tested analogues exhibited higher potency than compound **9**. However, all compounds demonstrated excellent selectivity toward *h*CAs, except for compound **25**.

The experimental evaluation of this series of compounds enabled us to derive sound structure-activity relationships (SARs) for this scaffold. The effect of the substitution in the 4-position can be highlighted, with activity decreasing in the order $CH_2 > O > S > NH$ for derivatives presenting a methyl group as the R^1 substituent (R^1═CH_3, R^2═H). Apparent exceptions observed in Table 3 arise from additional steric effects that alter the accessibility of the zinc ion (see below). Additionally, the stereochemistry of the C atom in the 3-position appears to play a more significant role as the size of the substituent increases. The *S* configuration is clearly preferred, as seen in **35** *vs.* **36** and **33** *vs.* **34**, especially when the R^1 group is large. However, enantioselectivity is lost with smaller substituents. For example, the *R* enantiomer of **26** is almost as active as the *S* enantiomer (**25**) on PsCA3 and is more selective over human isoforms. Full substitution of this atom is not well tolerated, producing suboptimal results (**27**).

Regarding substituent size, activity decreases when moving from methyl to ethyl (**22** and **23**) when X is a CH_2, while it does not change significantly when X is an oxygen atom. The *n*-butyl-substituted analog (**30**) exhibits the highest activity against PsCA3, as do the phenylethyl (**33**) and isopropyl (**11**) derivatives. However, other substitutions, such as *n*-propyl, phenyl, and cyclohexylmethyl, do not enhance inhibition.

This series of analogues was studied by molecular docking, using the previously described ensemble docking protocol and the MM-GBSA approach as a post-docking refinement. For analogues with one methyl substituent at C3 that differ only in the heteroatom at position 4 (**8–10**, **24–26**), the docking results are in line with the trend revealed by SAR analysis ($CH_2 > O > S > NH$) (Table S2, Supplementary Material). The highest docking score of the entire subset was reported when X is a

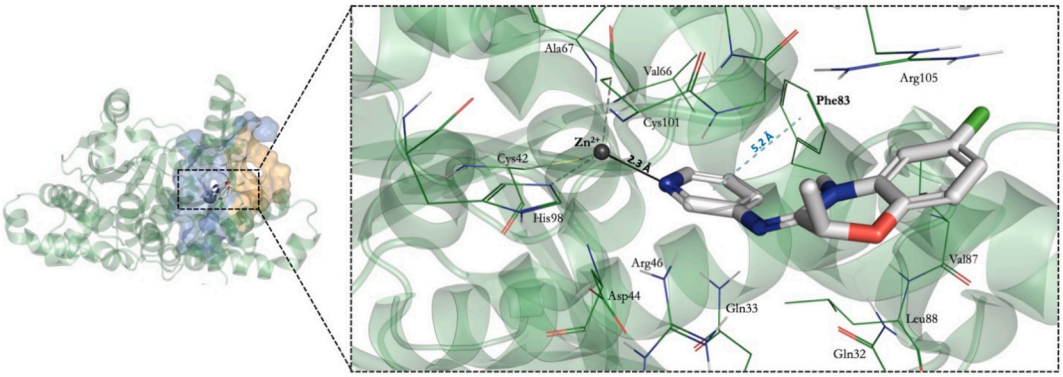

Fig. 2. Top-scored docking pose of compound **12** (silver sticks) into PsCA3 (PDB code: 6D2N, green cartoon), as obtained using docking protocol 1 (docking score = −6.517 kcal/mol; binding affinity$_{MM\text{-}GBSA}$ = −41.670 kcal/mol). On the left, the PsCA3 active site is visualized as a blue surface, with the selective valley region highlighted in orange. In the zoomed-in box on the right side, the zinc ion is shown as a gray sphere, and its molecular coordination by compound **12** is represented by a black line, while the π −T interaction with Phe83 as a cyan dotted line. Key residues within the active site are displayed as green lines. (For interpretation of the references to colour in this figure legend, the reader is referred to the web version of this article.)

Table 3
K_I values of benzoxazinone/dihydroquinolinone analogues and reference compound AAZ on *h*CAs I and II and PsCA3 through the stopped-flow CO_2 hydration assay.

Compound					K_I (μM)[a]		
			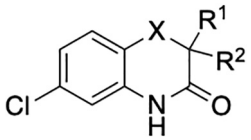				
N	X	Config	R^1	R^2	*h*CA I	*h*CA II	PsCA3
8	CH_2	*S*	CH_3	H	>100	>100	1.06
9	CH_2	*R*	CH_3	H	>100	>100	0.90
10	O		CH_3	H	>100	>100	1.15
11	O		$CH(CH_3)_2$	H	>100	92.5	0.91
22	CH_2		CH_2CH_3	H	>100	>100	60.0
23	CH_2	+[b]	CH_2CH_3	H	>100	>100	38.6
24	NH	*S*	CH_3	H	>100	>100	64.6
25	S	*S*	CH_3	H	6.76	4.86	4.21
26	S	*R*	CH_3	H	>100	>100	3.58
27	O		CH_3	CH_3	>100	>100	81.6
28	O	*S*	$CH_2CH_2CH_3$	H	>100	>100	8.94
29	O	*R*	$CH_2CH_2CH_3$	H	>100	>100	6.77
30	O		$CH_2CH_2CH_2CH_3$	H	>100	>100	0.98
31	O		$CH_2(CH_2)_5CH_3$	H	>100	>100	5.06
32	O		Ph	H	>100	>100	7.40
33	O	*S*	CH_2CH_2Ph	H	>100	>100	0.91
34	O	*R*	CH_2CH_2Ph	H	>100	>100	32.3
35	O	*S*	CH_2Cy[c]	H	>100	>100	7.87
36	O	*R*	CH_2Cy[c]	H	>100	>100	61.0
AAZ					0.25	0.012	0.076

[a] Mean from three different assays, by a stopped flow technique (errors were in the range of ±5–10 % of the reported values). Incubation: 8 h, r.t.
[b] The absolute configuration is unknown.
[c] Cy: cyclohexyl.

methylene group (**8**, **9**). The binding mode of the most potent inhibitor **9** in the PsCA3 active site is shown in Fig. 3. Despite the loss of aromatic interactions with Phe83, ligand **9** successfully binds to the zinc ion by properly orienting its chlorophenyl ring within the hydrophobic cavity as shown in Fig. 3 (Val66, Ala67, Phe83, Leu88, and Val87). On the contrary, the slightly less active *S*-enantiomer is not able to firmly localize within the active site. When X is an oxygen atom (**10**), slightly lower binding energetics (both docking score and binding affinity) are obtained. The introduction of a sulfur atom at position 4, as in compound **26**, leads to steric clashes with Gln33 and Gly102. Once again, the less potent *S* enantiomer (**25**) cannot be properly inserted into the catalytic site, even when a metal constraint is added to the docking procedure, similar to compound **24**, which does not reach the zinc ion.

Furthermore, the best docking results were obtained when the carbon at position 3 of the benzoxazinone scaffold was partially substituted. The docking results for **27**, which showed the worst *in vitro* β-CA inhibition, reveal that the compound cannot reach the catalytic zinc ion due to steric clashes between the methyl group and the too-close Phe83, Gly103, and Phe61 residues, even though the docking was performed in the IF-derived structure (Fig. S2, Supplementary Material).

Bearing this in mind, the best docking results were obtained for analogues with a single small non-bulky substituent, such as a methyl group (R^1═CH_3) and no substitution at R^2 position (R^2═H).

In silico studies help explain the activity of compounds **34**, **36**, **24**, and **27** that present the worst *in vitro* inhibitory activity within the series. Docking analysis, in fact, reveals their inability to dovetail with the active site (**24** and **27**) or to complex the zinc ion (**33** and **36**).

Compound **11** achieved a favorable docking score and binding affinity when analyzed using docking protocol 2, where the introduction of a metal constraint allowed the ligand to effectively coordinate the catalytic Zn^{2+} ion. In this binding mode, the molecule also establishes a relevant interaction with Gln33, a residue hypothesized to play a key role in PsCA3 catalysis by stabilizing the transition state during the hydration of CO_2 to HCO_3^-, as corroborated by site-directed mutagenesis studies.[64] Nevertheless, despite these favorable interactions, the presence of the isopropyl substituent forces the ligand into close proximity with Arg46, resulting in unfavorable steric contacts with this residue (Fig. S3, Supplementary Material).

3.5. Extending the β-CA inhibition panel

The promising inhibition data obtained for this series of compounds against PsCA3, along with their good pharmacokinetic profile (Table S3, Supplementary Material), prompted the exploration of a wider set of β-CAs from different microorganisms.

Thus, the most promising compounds of the benzoxazinone analogues (**8**–**11**, **24**, **25**, **30**, and **33**) were tested for enzyme inhibition against eight additional β-CAs, including those from *Porphyromonas gingivalis* (PgiCAβ), *Streptococcus mutans* (SmuCA), *Mycobacterium tuberculosis* (MtbCA3), *Vibrio cholerae* (VchAβ), *Burkholderia pseudomallei* (BpsCAβ), *Malassezia restrictans* (MreCA), *Malassezia globosa* (MgCA), and *Trichomonas vaginalis* (TvaCA1), covering a broad spectrum of bacteria, fungi, and parasites. Compound **25** was included in the analogue panel because its sulfur-containing scaffold and stereochemical configuration were essential to define SAR boundaries, despite its lower selectivity toward hCAs (see Table 4).

The analyzed compounds generally exhibited lower activity against the other tested β-CAs. The strongest inhibition was observed against

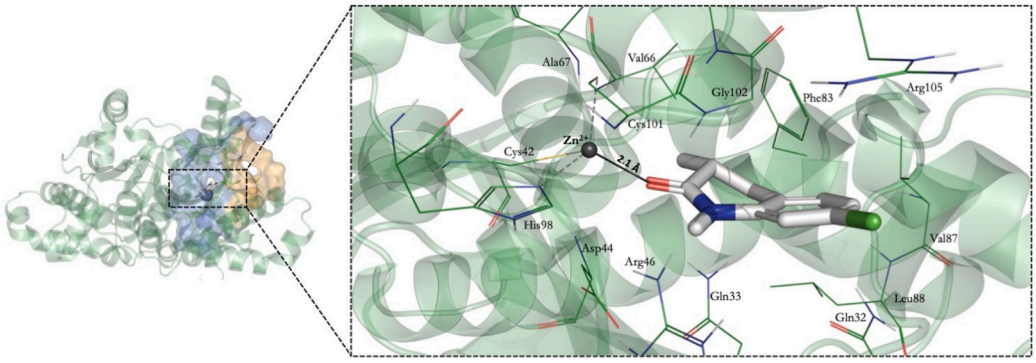

Fig. 3. Top-scored docking pose of compound **9** (silver sticks) into PsCA3 (PDB code 6D2N, green cartoon), as obtained using docking protocol 1 (docking score = −8.027 kcal/mol; binding affinity$_{MM\text{-}GBSA}$ = −42.470 kcal/mol). On the left, the PsCA3 active site is visualized as a blue surface, with the selective valley region highlighted in orange. In the zoomed-in box on the right side, the zinc ion is shown as a gray sphere, and its molecular coordination by compound **9** is represented by a black line. Key residues within the active site are displayed as green lines. (For interpretation of the references to colour in this figure legend, the reader is referred to the web version of this article.)

PgiCAβ, with all compounds displaying micromolar activity. In particular, compounds **10** and **25** showed activity comparable to that recorded for PsCA3. Additionally, the inhibition of PgiCAβ is significantly influenced by the stereochemistry at the C-3 position, though this dependence varies. For derivatives **8** and **9**, the *R* enantiomer is significantly more potent than the *S* enantiomer. However, when the X atom is replaced by sulfur, the enantioselectivity is inverted (**25** *vs.* **26**). Unlike PsCA3, there are no differences in potency depending on the substitution of the X atom. Most of the compounds exhibited activity against SmuCA, BpsCAβ, and VchAβ. Fungal (MreCA and MgCA) and parasitic (TvaCA1) β-CAs were less affected by this class of ligands. Notably, MtbCA3 was not inhibited by these compounds.

In summary, this class of compounds is a promising yet not optimized scaffold for developing new β-CAs inhibitors. On the other hand, the identified hits have fragment sizes and properties that align with the Rule of Three (Table S3, Supplementary Material), suggesting significant potential for optimization.

3.6. Structural analysis of microbial β-CAs bound to compound 9

To gain a better insight into the activity data against microbial β-CAs and to rationalize the observed isoform selectivity, structure-based studies were performed focusing on the binding of the most active ligand **9** to the tested enzymes. For this purpose, we collected the available 3D coordinates of the different proteins from the PDB and AlphaFold repositories. The structures of VchCAβ and PgiCAβ were obtained by homology modeling as described in the experimental section. An IF docking was applied to dock compound **9** into the narrow β-CA active sites. In fact, the simple docking calculations could not find a suitable binding pose of the ligand in the active site, without adapting the protein to fit the ligand, as we have experienced with this class of enzymes.[19,20] Finally, the best IF docking pose was considered for each protein to evaluate the binding mode of ligand **9** and to describe the characteristics of the active site using the SiteMap tool.

In all studied enzymes, similar contacts are observed: the carbonyl oxygen coordinates the zinc ion, while the amide hydrogen atom is engaged in a hydrogen bond (HB) with an aspartic acid residue, except for VchCAβ and MtbCA3. Additionally, the aromatic ring establishes a π-π-interaction with a phenylalanine/tyrosine residue for PgiCAβ, VchCAβ, MtbCA3, MgCA, and MreCA (Fig. S4, Supplementary Material).

The binding pocket was analyzed by positioning a probe on defined site points and employing van der Waals (vdW) and electrostatic interactions to create a field map. In Table 5, the total (accessible solvent) surface, HB acceptor, HB donor, and hydrophobic surfaces of the binding sites were reported.

The most remarkable finding from this study is that the proteins for which compound **9** showed some inhibitory activity, albeit weak, had a total surface area exceeding 658 Å^2, which is directly related to the dimensions of the hydrogen bond donor and acceptor surfaces. A visual analysis of the site map results revealed that, in the four enzymes for which compound **9** is inactive, the hydrophobic area is concentrated closer to the zinc ion in the inner part of the site than in the other enzymes, irrespective of its dimensions (Fig. S5, Supplementary Material).

Table 5
The total Surface, HB acceptor, HB donor, and Hydrophobic surface areas (Å^2) calculated with SiteMap for the microbial β-CA binding sites. The corresponding K_I of compound **9** is reported as a reference.

β-CAs	K_I (μM) of 9	Surface	HB acceptor	HB donor	Hydrophobic
PsCA3	*0.90*	*812.587*	*216.719*	*296.982*	*202.595*
PgiCAβ	*3.19*	*926.680*	*196.120*	*368.666*	*197.376*
BpsCAβ	*36.1*	*658.029*	*222.155*	*265.776*	*105.911*
VchCAβ	*41.48*	*684.764*	*202.878*	*334.147*	*170.225*
SmuCA	*66.9*	*741.673*	*172.597*	*318.963*	*157.665*
MgCA	>100	596.077	151.866	205.754	198.514
MreCA	>100	621.685	197.408	248.220	197.616
MtbCA3	>100	626.637	91.463	368.167	71.985
TvaCA1	>100	382.609	84.598	119.317	66.466

To further emphasize the structural differences in the studied β-CAs, the amino acids in the active site located up to 5 Å from **9** were aligned, as illustrated in Fig. 4. In chain A, the catalytic triad (two cysteines and a histidine) is conserved, together with Asp44 and Arg46 of PsCA3; all other residues vary from one enzyme to another. In chain B, Gln33 is conserved in bacterial (with the exception of SmuCA) and in fungal enzymes (MreCA and MgCA), whereas Phe83 is usually replaced by tyrosine. The protozoal chain B of TvaCA1 exhibits the least similarity to the others.

4. Conclusions

This study showcases a successful compound repurposing approach leveraging advanced structure-based computational techniques to identify novel inhibitors of microbial β-CAs, with a primary focus on PsCA3 from *P. aeruginosa*. A consensus docking pipeline, integrated with binding energy calculations and *in vitro* validation, enabled the selection of potent and selective compounds.

Among the hits, the benzoxazinone/dihydroquinolinone scaffold emerged as a particularly promising chemical framework, offering an optimal combination of biological activity, selectivity over human CAs, synthetic tractability, and structural flexibility. Further evaluation against a broader panel of β-CAs confirmed the potential of this class of compounds, especially compound **9**, as microbial β-CA inhibitors, particularly against bacterial enzymes. Moreover, the fragment-like nature of identified compounds engenders ample opportunity for optimization.

Structural analysis revealed the critical role of protein moulding in accommodating ligands within narrow or occluded active sites, as observed in PsCA3. These findings underscore the need to consider Induced Fit effects during the design and optimization of β-CA inhibitors.

Table 4
K_I values of selected compounds and reference compound AAZ on a panel of β-CAs from bacteria (PgiCAβ, SmuCA, MtbCA3, VchCAβ, BpsCAβ), fungi (MreCA, MgCA), and the protozoan *T. vaginalis* (TvaCA1), compared with *h*CA I, *h*CA II, and PsCA3 through the stopped-flow CO_2 hydration assay.

N	K_I (μM)[a]										
	*h*CA I	*h*CA II	PsCA3	PgiCAβ	SmuCA	MtbCA3	VchCAβ	BpsCAβ	MreCA	MgCA	TvaCA1
8	>100	>100	1.06	11.3	78.27	>100	47.1	33.1	>100	87.4	>100
9	>100	>100	0.90	3.19	66.9	>100	41.4	36.1	>100	>100	>100
10	>100	>100	1.15	2.21	67.0	>100	28.9	>100	10.7	>100	>100
11	>100	92.50	0.92	17.5	74.8	>100	>100	75.3	>100	>100	41.9
25	6.76	4.86	4.21	3.59	>100	>100	>100	>100	>100	>100	>100
26	>100	>100	3.58	14.1	68.6	>100	47.0	88.0	>100	80.8	28.9
30	>100	>100	0.98	14.6	65.0	93.05	>100	59.1	>100	>100	>100
33	>100	>100	0.91	11.5	67.9	>100	>100	63.6	14.5	81.72	>100
AAZ	0.250	0.012	0.08	0.21	0.34	0.1	0.45	0.75	0.1	74	0.39

[a] Mean from 3 different assays, by a stopped flow technique (errors were in the range of ±5–10 % of the reported values). Incubation: 8 h, r.t.

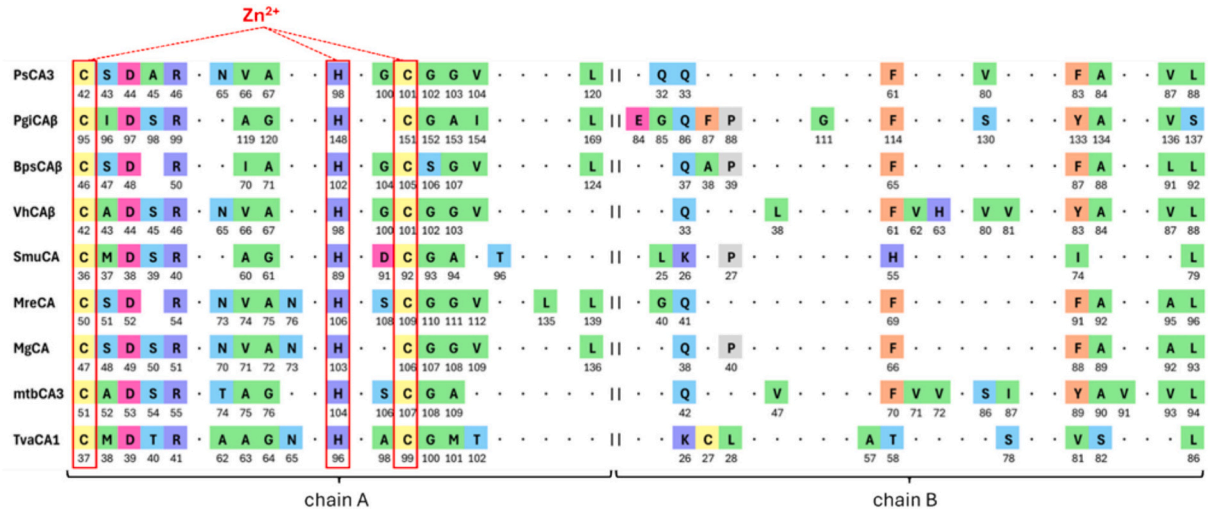

Fig. 4. Sequence alignment of microbial β-CAs, focusing on residues ranging 5 Å from **9**.

In summary, this work lays the groundwork for the rational development of selective β-CA inhibitors as potential antimicrobial agents. By targeting underexplored enzymes, such as microbial β-CAs, these findings offer valuable insight into alternative therapeutic strategies for addressing antimicrobial resistance and expanding the antibiotic arsenal. Among the active fragments, compound **9** emerged as the most suitable ligand for structural investigation, guiding the identification of benzoxazinone/dihydroquinolinone as privileged scaffolds for further optimization.

CRediT authorship contribution statement

Anna Rita Tondo: Writing – original draft, Visualization, Methodology, Investigation, Formal analysis. **Marialuigia Fantacuzzi:** Writing – original draft, Visualization, Methodology, Investigation, Formal analysis. **Simone Carradori:** Project administration, Funding acquisition. **Ilaria D'Agostino:** Validation, Investigation, Formal analysis. **Andrea Angeli:** Validation, Investigation, Formal analysis. **Claudiu T. Supuran:** Supervision, Funding acquisition. **Clemente Capasso:** Resources, Funding acquisition. **Nicola Gambacorta:** Software. **Luca Piemontese:** Resources, Data curation. **Antonio Laghezza:** Resources, Data curation. **Orazio Nicolotti:** Writing – review & editing, Supervision. **Paolo Tortorella:** Writing – review & editing, Resources, Conceptualization. **Mariangela Agamennone:** Writing – review & editing, Writing – original draft, Supervision, Conceptualization.

Declaration of competing interest

The authors declare that they have no known competing financial interests or personal relationships that could have appeared to influence the work reported in this paper.

Acknowledgements

This work was supported by a grant from the Italian Ministry of University and Research for financial support under the FISR program, project FISR_04819 BacCAD to C.T.S., C.C., and S.C..This article is based upon work from COST Action EURESTOP, CA21145, supported by COST (European Cooperation in Science and Technology) to S.C. and I.D.A..

Appendix A. Supplementary data

Supplementary data to this article can be found online at https://doi.org/10.1016/j.bmc.2025.118542.

Data availability

Data will be made available on request.

References

1. Murray CJL, Ikuta KS, Sharara F, et al. Global burden of bacterial antimicrobial resistance in 2019: a systematic analysis. *Lancet*. 2022;399(10325):629–655. https://doi.org/10.1016/S0140-6736(21)02724-0.
2.. Antimicrobial resistance. Accessed July 7, 2025. https://www.who.int/news-room/fact-sheets/detail/antimicrobial-resistance.
3.. Dance A. Five ways science is tackling the antibiotic resistance crisis. *Nature*. 2024;632(8025):494–496. https://doi.org/10.1038/d41586-024-02601-4.
4. Naghavi M, Vollset SE, Ikuta KS, et al. Global burden of bacterial antimicrobial resistance 1990–2021: a systematic analysis with forecasts to 2050. *Lancet*. 2024;404(10459):1199–1226. https://doi.org/10.1016/S0140-6736(24)01867-1.
5. Rosamond J, Allsop A. Harnessing the power of the genome in the search for new antibiotics. *Science*. 2000;287(5460):1973–1976. https://doi.org/10.1126/science.287.5460.1973.
6. Halawa EM, Fadel M, Al-Rabia MW, et al. Antibiotic action and resistance: updated review of mechanisms, spread, influencing factors, and alternative approaches for combating resistance. *Front Pharmacol*. 2024:14. https://doi.org/10.3389/fphar.2023.1305294.
7. Supuran CT. An overview of novel antimicrobial carbonic anhydrase inhibitors. *Expert Opin Ther Targets*. 2023;27(10):897–910. https://doi.org/10.1080/14728222.2023.2263914.
8. Supuran CT. Structure and function of carbonic anhydrases. *Biochem J*. 2016;473(14):2023–2032. https://doi.org/10.1042/BCJ20160115.
9. Nocentini A, Supuran CT. Carbonic anhydrases: an overview. In: *Carbonic anhydrases: biochemistry and pharmacology of an evergreen pharmaceutical target*. 2019:3–16. https://doi.org/10.1016/B978-0-12-816476-1.00001-0.
10. Supuran Claudiu T, Clemente Capasso. Antibacterial carbonic anhydrase inhibitors: an update on the recent literature. *Expert Opin Ther Pat*. 2020. https://doi.org/10.1080/13543776.2020.1811853. Published online August 19.
11. Del Prete S, Vullo D, De Luca V, et al. Anion inhibition profiles of α-, β- and γ-carbonic anhydrases from the pathogenic bacterium vibrio cholerae. *Bioorg Med Chem*. 2016;24(16):3413–3417. https://doi.org/10.1016/j.bmc.2016.05.029.
12. Lotlikar SR, Kayastha BB, Vullo D, et al. Pseudomonas aeruginosa β-carbonic anhydrase, psCA1, is required for calcium deposition and contributes to virulence. *Cell Calcium*. 2019;84, 102080. https://doi.org/10.1016/j.ceca.2019.102080.
13. Campestre C, De Luca V, Carradori S, et al. Carbonic anhydrases: new perspectives on protein functional role and inhibition in helicobacter pylori. *Front Microbiol*. 2021:12. https://doi.org/10.3389/fmicb.2021.629163.
14. Capasso C, Supuran CT. Carbonic anhydrase and bacterial metabolism: a chance for antibacterial drug discovery. *Expert Opin Ther Pat*. 2024;34(6):465–474. https://doi.org/10.1080/13543776.2024.2332663.
15. Benito G, D'Agostino I, Carradori S, et al. Erlotinib-Containing Benzenesulfonamides As Anti- *Helicobacter Pylori* Agents Through Carbonic Anhydrase Inhibition. *Future Med Chem*. 2023;15(20):1865–1883. https://doi.org/10.4155/fmc-2023-0208.
16. Urbanski LJ, Bua S, Angeli A, et al. Sulphonamide inhibition profile of Staphylococcus aureus β-carbonic anhydrase. *J Enzyme Inhib Med Chem*. 2020;35(1):1834–1839. https://doi.org/10.1080/14756366.2020.1826942.
17. Abutaleb NS, Elkashif A, Flaherty DP, Seleem MN. In vivo antibacterial activity of acetazolamide. *Antimicrob Agents Chemother*. 2021;65(4). https://doi.org/10.1128/AAC.01715-20.
18.. Colquhoun Jennifer M, Marjan Farokhyfar, Anderson Alexander C, et al. Collateral changes in cell physiology associated with ADC-7 β-lactamase expression in

Acinetobacter baumannii. *Microbiol Spectr*. 2023. https://doi.org/10.1128/spectrum.04646-22. Published online April 19.
19. Fantacuzzi M, D'Agostino I, Carradori S, et al. Benzenesulfonamide derivatives as *Vibrio cholerae* carbonic anhydrases inhibitors: a computational-aided insight in the structural rigidity-activity relationships. *J Enzyme Inhib Med Chem*. 2023;38(1):2201402. https://doi.org/10.1080/14756366.2023.2201402.
20. Marinacci B, D'Agostino I, Angeli A, et al. Inhibition of Pseudomonas aeruginosa Carbonic Anhydrases, Exploring Ciprofloxacin Functionalization Toward New Antibacterial Agents: An In-Depth Multidisciplinary Study. *J Med Chem*. 2024;67(21):19077–19102. https://doi.org/10.1021/acs.jmedchem.4c01555.
21. Miller WR, Arias CA. ESKAPE pathogens: antimicrobial resistance, epidemiology, clinical impact and therapeutics. *Nat Rev Microbiol*. 2024;22(10):598–616. https://doi.org/10.1038/s41579-024-01054-w.
22. WHO bacterial priority pathogens list, 2024: Bacterial pathogens of public health importance to guide research, development and strategies to prevent and control antimicrobial resistance. Accessed July 7, 2025. https://www.who.int/publications/i/item/9789240093461.
23. Lotlikar SR, Hnatusko S, Dickenson NE, Choudhari SP, Picking WL, Patrauchan MA. Three functional β-carbonic anhydrases in Pseudomonas aeruginosa PAO1: Role in survival in ambient air. *Microbiol U K*. 2013;159(8):1748–1759. https://doi.org/10.1099/mic.0.066357-0.
24. Pinard MA, Lotlikar SR, Boone CD, et al. Structure and inhibition studies of a type II beta-carbonic anhydrase psCA3 from *Pseudomonas aeruginosa*. *Bioorg Med Chem*. 2015;23(15):4831–4838. https://doi.org/10.1016/j.bmc.2015.05.029.
25. Schrödinger Release, 2021-2: Maestro, Glide, LigPrep, Phase, MacroModel, SiteMap, New York, NY, 2021.
26. Murray AB, Aggarwal M, Pinard M, et al. Structural Mapping of Anion Inhibitors to β-Carbonic Anhydrase psCA3 from Pseudomonas aeruginosa. *ChemMedChem*. 2018;13(19):2024–2029. https://doi.org/10.1002/cmdc.201800375.
27. Berman HM, Westbrook J, Feng Z, et al. The Protein Data Bank. *Nucleic Acids Res*. 2000;28(1):235–242.
28. Rowlett RS. Structure and catalytic mechanism of β-carbonic anhydrases. *Subcell Biochem*. 2014;75:53–76. https://doi.org/10.1007/978-94-007-7359-2_4.
29. Lu C, Wu C, Ghoreishi D, et al. OPLS4: Improving Force Field Accuracy on Challenging Regimes of Chemical Space. *J Chem Theory Comput*. 2021;17(7):4291–4300. https://doi.org/10.1021/acs.jctc.1c00302.
30. Friesner RA, Banks JL, Murphy RB, et al. Glide: a new approach for rapid, accurate docking and scoring. 1. Method and assessment of docking accuracy. *J Med Chem*. 2004;47(7):1739–1749. https://doi.org/10.1021/jm0306430.
31. Halgren TA, Murphy RB, Friesner RA, et al. Glide: a new approach for rapid, accurate docking and scoring. 2. Enrichment factors in database screening. *J Med Chem*. 2004;47(7):1750–1759. https://doi.org/10.1021/jm030644s.
32. Genheden S, Ryde U. The MM / PBSA and MM / GBSA methods to estimate ligand-binding affinities. Published online 2015.
33. Angeli A, Ferraroni M, Pinteala M, et al. Crystal structure of a tetrameric type II β-carbonic anhydrase from the pathogenic bacterium burkholderia pseudomallei. *Molecules*. 2020;25(10). https://doi.org/10.3390/molecules25102269.
34. Varadi M, Bertoni D, Magana P, et al. AlphaFold Protein Structure Database in 2024: providing structure coverage for over 214 million protein sequences. *Nucleic Acids Res*. 2024;52(D1):D368–D375. https://doi.org/10.1093/nar/gkad1011.
35. AlphaFold Protein Structure Database. Accessed July 8, 2025. https://alphafold.ebi.ac.uk/.
36. UniProt: the Universal Protein Knowledgebase in 2023. Accessed May 2, 2025. https://europepmc.org/article/MED/36408920.
37. Schrödinger Release 2025-1: Maestro, Epik, Glide, MacroModel, Prime, Induced Fit Docking protocol, Protein Preparation Workflow, LigPrep, SiteMap, Schrödinger, LLC, New York, NY, 2025.
38. Camacho C, Coulouris G, Avagyan V, et al, BLAST+. architecture and applications. *BMC Bioinformatics*. 2009;10(1):421. https://doi.org/10.1186/1471-2105-10-421.
39. Covarrubias AS, Bergfors T, Jones TA, Högbom M. Structural mechanics of the pH-dependent activity of β-carbonic anhydrase from Mycobacterium tuberculosis. *J Biol Chem*. 2006;281(8):4993–4999. https://doi.org/10.1074/jbc.M510756200.
40. Khalifah RG. The Carbon Dioxide Hydration Activity of Carbonic Anhydrase: I. Stop-flow kinetic studies on the native human isoenzymes B and C. *J Biol Chem*. 1971;246(8):2561–2573. https://doi.org/10.1016/S0021-9258(18)62326-9.
41. Pinard M, Lotlikar S, Patrauchan MA, McKenna R. Preliminary X-ray crystallographic analysis of β-carbonic anhydrase psCA3 from Pseudomonas aeruginosa. *Acta Crystallograph Sect F Struct Biol Cryst Commun*. 2013;69(8):891–894. https://doi.org/10.1107/S1744309113017594.
42. Angeli A, Pinteala Mariana, Maier, Stelian S, et al. Inhibition of α-, β-, γ-, δ-, ζ- and η-class carbonic anhydrases from bacteria, fungi, algae, diatoms and protozoans with famotidine. *J Enzyme Inhib Med Chem*. 2019;34(1):644–650. https://doi.org/10.1080/14756366.2019.1571273.
43. Nicolotti O, Miscioscia TF, Leonetti F, Muncipinto G, Carotti A. Screening of Matrix Metalloproteinases Available from the Protein Data Bank: Insights into Biological Functions, Domain Organization, and Zinc Binding Groups. *J Chem Inf Model*. 2007;47(6):2439–2448. https://doi.org/10.1021/ci700119r.
44. Nicolotti O, Catto M, Giangreco I, et al. Design, synthesis and biological evaluation of 5-hydroxy, 5-substituted-pyrimidine-2,4,6-triones as potent inhibitors of gelatinases MMP-2 and MMP-9. *Eur J Med Chem*. 2012;58:368–376. https://doi.org/10.1016/j.ejmech.2012.09.036.
45. Rubino MT, Agamennone M, Campestre C, et al. Biphenyl Sulfonylamino Methyl Bisphosphonic Acids as Inhibitors of Matrix Metalloproteinases and Bone Resorption. *ChemMedChem*. 2011;6(7). https://doi.org/10.1002/cmdc.201000540.
46. Di Pizio A, Agamennone M, Laghezza A, Loiodice F, Tortorella P. Mimic catechins to develop selective MMP-2 inhibitors. *Monatshefte Chem*. 2018;149(7). https://doi.org/10.1007/s00706-018-2237-4.
47. Luisi G, Angelini G, Gasbarri C, et al. Dual targeting of cancer-related human matrix metalloproteinases and carbonic anhydrases by chiral *N* -(biarylsulfonyl)-phosphonic acids. *J Enzyme Inhib Med Chem*. 2017;32(1):1260–1264. https://doi.org/10.1080/14756366.2017.1378192.
48. Tauro M, Loiodice F, Ceruso M, Supuran CT, Tortorella P. Bioorganic & Medicinal Chemistry Letters Dual carbonic anhydrase / matrix metalloproteinase inhibitors incorporating bisphosphonic acid moieties targeting bone tumors. *Bioorg Med Chem Lett*. 2014;24(12):2617–2620. https://doi.org/10.1016/j.bmcl.2014.04.077.
49. Tauro M, Loiodice F, Ceruso M, Supuran CT, Tortorella P. Arylamino bisphosphonates: Potent and selective inhibitors of the tumor-associated carbonic anhydrase XII. *Bioorg Med Chem Lett*. 2014;24(8):1941–1943. https://doi.org/10.1016/j.bmcl.2014.03.001.
50. Piemontese L, Fracchiolla G, Carrieri A, et al. Design, synthesis and biological evaluation of a class of bioisosteric oximes of the novel dual peroxisome proliferator-activated receptor α/γ ligand LT175. *Eur J Med Chem*. 2015;90:583–594. https://doi.org/10.1016/j.ejmech.2014.11.044.
51. Poliseno V, Chaves S, Brunetti L, et al. Derivatives of Tenuazonic Acid as Potential New Multi-Target Anti-Alzheimer's Disease Agents. *Biomolecules*. 2021;11(1). https://doi.org/10.3390/biom11010111.
52. Tricarico D, Mele A, Camerino GM, et al. Molecular Determinants for the Activating/Blocking Actions of the 2*H*-1,4-Benzoxazine Derivatives, a Class of Potassium Channel Modulators Targeting the Skeletal Muscle KATP Channels. *Mol Pharmacol*. 2008;74(1):50–58. https://doi.org/10.1124/mol.108.046615.
53. Piemontese L, Laghezza A, Fracchiolla G, Carbonara G, Tortorella P, Loiodice F. An efficient synthesis of the optically active isomers of 2*H*-1,4-benzoxazine derivatives, novel KATP channel modulators. *Tetrahedron Asymmetry*. 2013;24(13):791–795. https://doi.org/10.1016/j.tetasy.2013.05.027.
54. Rowlett RS. Structure and catalytic mechanism of the β-carbonic anhydrases. *Biochim Biophys Acta BBA - Proteins Proteomics*. 2010;1804(2):362–373. https://doi.org/10.1016/j.bbapap.2009.08.002.
55. Leuci R, Brunetti L, Laghezza A, et al. A New Series of Aryloxyacetic Acids Endowed with Multi-Target Activity towards Peroxisome Proliferator-Activated Receptors (PPARs), Fatty Acid Amide Hydrolase (FAAH), and Acetylcholinesterase (AChE). *Molecules*. 2022;27(3):958. https://doi.org/10.3390/molecules27030958.
56. Tauro M, Laghezza A, Loiodice F, Agamennone M, Campestre C, Tortorella P. Arylamino methylene bisphosphonate derivatives as bone seeking matrix metalloproteinase inhibitors. *Bioorg Med Chem*. 2013;21(21):6456–6465. https://doi.org/10.1016/j.bmc.2013.08.054.
57. Laghezza A, Piemontese L, Brunetti L, et al. (2-Aminobenzothiazole)-Methyl-1,1-bisphosphonic acids: Targeting matrix metalloproteinase 13 inhibition to the bone. *Pharmaceuticals*. 2021;14(2). https://doi.org/10.3390/ph14020085.
58. Laghezza A, Piemontese L, Brunetti L, et al. Bone-Seeking Matrix Metalloproteinase Inhibitors for the Treatment of Skeletal Malignancy. *Pharmaceuticals*. 2020;13(6):113. https://doi.org/10.3390/ph13060113.
59. Tauro M, Laghezza A, Loiodice F, et al. Catechol-based matrix metalloproteinase inhibitors with additional antioxidative activity. *J Enzyme Inhib Med Chem*. 2016;31. https://doi.org/10.1080/14756366.2016.1217853.
60. Rahman F, Nguyen ,Tra-Mi, Adekoya ,Olayiwola A., et al. Inhibition of bacterial and human zinc-metalloproteases by bisphosphonate- and catechol-containing compounds. *J Enzyme Inhib Med Chem*. 2021;36(1):819-830. doi:10.1080/14756366.2021.1901088.
61. Holloway GA, Baell JB. New substructure filters for removal of pan assay interference compounds (PAINS) from screening libraries and for their exclusion in bioassays. *J Med Chem. Published online*. 2010.
62. Bozdag M, Bua Silvia, Osman, Sameh M. AlOthman ,Zeid, and Supuran CT. Carbonic anhydrase I, II, IV and IX inhibition with a series of 7-amino-3,4-dihydroquinolin-2(1H)-one derivatives. *J Enzyme Inhib Med Chem*. 2017;32(1):885–892. https://doi.org/10.1080/14756366.2017.1337759.
63. Gambacorta N, Gasperi V, Guzzo T, et al. Exploring the 1,3-benzoxazine chemotype for cannabinoid receptor 2 as a promising anti-cancer therapeutic. *Eur J Med Chem*. 2023;259:115647. https://doi.org/10.1016/j.ejmech.2023.115647.
64. Aggarwal M, Chua TK, Pinard MA, Szebenyi DM, McKenna R. Carbon Dioxide "Trapped" in a β-Carbonic Anhydrase. *Biochemistry*. 2015;54(43):6631–6638. https://doi.org/10.1021/acs.biochem.5b00987.